



# STUDY AND MODELING OF NEAR-FAULT STRONG MOTIONS OCCURRING FREQUENTLY IN SERIES OF ACTIVE CRUSTAL EARTHQUAKES

Toru ISHII

Member, Dr. Eng., Chief Research Engineer, Institute of Technology, Shimizu Corporation,  
Tokyo, Japan, [tokyo@shimz.co.jp](mailto:tokyo@shimz.co.jp)

**ABSTRACT:** This study investigated the frequent near-fault strong motions recorded during active series of inland crustal earthquakes using sorted and ranked pseudo-velocity response spectra and ranked response spectral ratios to realize performance-based design consideration for buildings. The impact of repeating strong motions on building responses could be determined by multiplying the response spectra of the design-standard earthquake motions or the target spectra by the proposed ranked response spectral ratios.

**Keywords:** Crustal earthquake, Active fault, Near-fault region, Strong motion, Repetition, Design

## 1. INTRODUCTION

After a large earthquake, several aftershocks are selectively generated along the source fault plane. In particular, a series of active crustal earthquakes such as the 2004 Chuetsu Earthquake in Niigata Prefecture, Japan, along with its aftershocks<sup>1)</sup> and the 2016 Kumamoto Earthquakes<sup>2)</sup>, caused several earthquake motions of the largest class near the epicenters. Moreover, the ground motion of a foreshock or an aftershock may exceed that of the main shock, depending on the location<sup>1), 2)</sup>.

The 2004 Chuetsu Earthquake in Niigata Prefecture occurred at 17:56 on October 23 (JST), 2004 with a magnitude of  $M$  6.8 and a maximum seismic intensity of 7<sup>1)</sup>. However, three aftershocks of  $M$  6.0 or larger occurred within just one hour of the stated earthquake, and ground motions of the largest class with a maximum seismic intensity of 6-lower to 6-upper were repeated in the near-fault region<sup>1)</sup>. The 2016 Kumamoto Earthquakes is a general term used to denote the series of seismic activities that occurred along the active fault zone from the Takano–Shirahata segment of the Hinagu fault zone to the Futagawa segment of the Futagawa fault zone with repeated strong motions occurring in the near-fault region<sup>2)</sup>. Moreover, strong motions with a seismic intensity of 7 occurred twice at the Mashiki Town in the Kumamoto Prefecture—located in the vicinity of the active fault—within less than 28 h owing to the events of  $M$  6.5 at 21:26 on April 14 and  $M$  7.3 at 1:25 on April 16 (JST)<sup>2)</sup>. Surprisingly, the number of series of earthquakes was extremely large in every case, even when compared with major earthquakes that occurred inland and along the coast of Japan in recent years<sup>1), 2)</sup>.

During such active seismic activity, time for repairing buildings or transferring valuables that are difficult to transport is insufficient. Conventionally, earthquake-resistant design and analysis of buildings rarely consider the serial impact of the largest strong motions caused in the near-fault region

of such serial seismic activity, which selectively and inevitably occur under limited conditions. A series of active crustal earthquakes results in a series of strong motions in the near-fault region, and is thus, required for evaluation. However, seismic observation in the vicinity of epicenters are almost unavailable. Consequently, the data required for design and investigation are yet to be analyzed to date.

In recent years, high-density seismic observation networks (K-NET and KiK-net)<sup>3)</sup> have been established across Japan for obtaining high-quality seismic observations in the near-fault region of such frequent seismic activities, thus facilitating their analysis and investigations for the first time. Consequently, a series of strong motions observed at very high frequencies can be analyzed based on their periodic characteristics for performance-based design and assessment of buildings. This is done with consideration of whether the largest seismic motions actually repeat at the same site and determining the relative intensity of other strong motions in the near-fault region for predominant typical ground motions. More importantly, the amplitude of the largest expected ground motion requires accurate evaluation and should be reflected in the design-standard earthquake motion. In general, the structural safety problems of the target building can be eradicated via elastic designs and sufficient margin. However, for instance, a plastic member or joint component can cause problems such as progressive rupture in which plastic deformation progresses over a period owing to the largest series of seismic motions. Thus, the presence or absence of such components should be confirmed during the design phase. In addition, the various building performances, in addition to safety, require consideration. Moreover, the response amplitude as well as the response duration should be considered based on the desired performance of the building when several aftershocks repeat frequently, even if the duration of each earthquake motion is not very long. Although the magnitude of these problems depends on the structural characteristics of buildings and structures and their required performance, the present author suggests an idea that could be properly addressed for its active representation in the performance-based design.

Therefore, the strong motion surface-observations in the near-fault region during the serial seismic activities of the 2004 Chuetsu Earthquake in Niigata Prefecture as well as its aftershocks and those of the 2016 Kumamoto Earthquakes were analyzed in this study. Furthermore, the actual strong motions in the near-fault region was examined, and a modeling measure was proposed to sustain strong motions and ensure adequate design and assessment of buildings. The data and methods of this study are detailed in Chapter 2, and the actual conditions of strong motions in the vicinity of the epicenter are presented in Chapters 3 and 4, with further discussion in Chapter 5. Thereafter, the model proposed for sustaining repeated strong motions is described in Chapter 6. Finally, the study is concluded in Chapter 7.

In this study, the 2004 Chuetsu Earthquake in Niigata Prefecture and its aftershock activity are collectively referred to as the “Chuetsu Earthquakes,” and the series of seismic activity of the 2016 Kumamoto Earthquakes is referred to as the “Kumamoto Earthquakes.”

## **2. DATA AND METHODS USED IN THIS STUDY**

The data and methods used in the current study are explained with the flowchart in Fig. 1.

In this study, among the public data of K-NET and KiK-net of the National Research Institute for Earth Science and Disaster Resilience, the three components (NS: north-south, EW: east-west, and UD: up-down) of the acceleration time histories of the surface ground motions recorded at the strong-motion observation stations in the near-fault region of the Chuetsu and Kumamoto Earthquakes were examined.

The existence of multiple active faults is known around the seismic activity area of the Chuetsu earthquakes, and these earthquakes were probably caused by the northern part of the fault zone along the western edge of the Muika-machi basin. Moreover, a majority of the source fault planes are underground and distributed in a three-dimensionally complex form<sup>1)</sup>. On the contrary, a clear surface fault appeared during the Kumamoto Earthquakes mainly from the Takano–Shirahata segment of the Hinagu fault zone to the Futagawa segment of the Futagawa fault zone. A majority of the seismic activity was distributed along a plane that was inclined deeply northwest from this active fault zone<sup>2)</sup>. Although the near-fault region varied depending on the individual earthquake, the observation stations located approximately 10 km from each major three-dimensional seismic activity space<sup>1), 2)</sup> were selected for

investigating the effect of the entire series of seismic activity occurring in the area along the active faults on the seismic motion, including all the stations directly above the space.

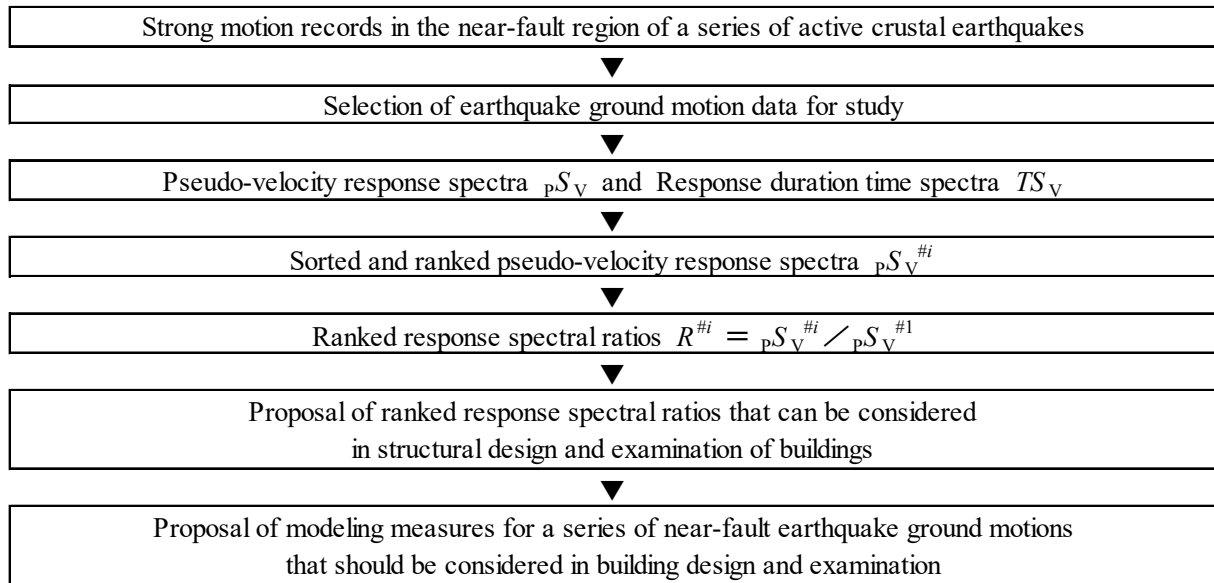


Fig. 1 Flowchart of this study

The study period was from 17:56 on October 23 to 24:00 on December 31, 2004 for the Chuetsu earthquakes and from 21:26 on April 14 to 24:00 on June 30, 2016 for the Kumamoto Earthquakes, including the period of seismic activity. The volume and quality of earthquake observation data acquired from the seismic activity area during the target period at each target observation station was comprehensively assessed. Afterward, all the three-component ground motion records with a maximum value for at least one component as  $100 \text{ cm/s}^2$  or more were selected without omission as a guideline for studying large-amplitude earthquake motions in the near-fault region. Notably, the observation data for KMMH14 (Toyono) of the earthquake at 1:44 on April 16, 2016 was included in the same record as the data of the earthquake immediately after selection, regardless of its maximum value being less than  $100 \text{ cm/s}^2$ .

The Chuetsu and Kumamoto Earthquakes are illustrated in Fig. 2, where the selected observation stations<sup>3)</sup> are marked by dark blue squares, the epicenters of earthquakes<sup>4)</sup> are represented by circles, and the surface traces of the surrounding active faults<sup>5)</sup> are denoted by green lines. In particular, the date of occurrence and  $M$ <sup>4)</sup> were included in the figure for each earthquake with a magnitude  $M$  of 6.0 or larger and that caused almost the largest ground motion in the surrounding area. As discussed earlier, the underground distribution of the seismic activity of the Chuetsu Earthquakes was complicated, and the relationship with the surrounding active faults was unclear at certain instances. On the contrary, the main body of the underground fault plane of the Kumamoto Earthquakes inclined deeply toward the northwest from the surface traces of the Takano–Shirahata segment of the Hinagu fault zone to the Futagawa segment of the Futagawa fault zone. Moreover, the epicenters of a majority of seismic activities were distributed on the northwest side of the surface trace. As depicted in Fig. 2, seven stations for the Chuetsu earthquakes and five stations for the Kumamoto Earthquakes were selected as target stations in this study. In particular, KMMH14 (Toyono) and KMMH16 (Mashiki) are located close to the surface faults appearing in the Kumamoto Earthquakes. Further, the sites of NIG028 (Nagaoka branch) and NIGH01 (Nagaoka) are adjacent to each other.

All the earthquake ground motion records used in the current study<sup>3), 4)</sup> are presented in Table 1. In particular, the items corresponding to earthquakes with a magnitude  $M$  of 6.0 or larger are marked in light blue, and the items for KMMH14 (Toyono) and KMMH16 (Mashiki) located in the vicinity of the above-mentioned surface fault are highlighted in green. The number of earthquakes selected for study

varied depending on the location of the observation station; 7–29 earthquakes were selected at each station, as reflected in the bottom row of the table.

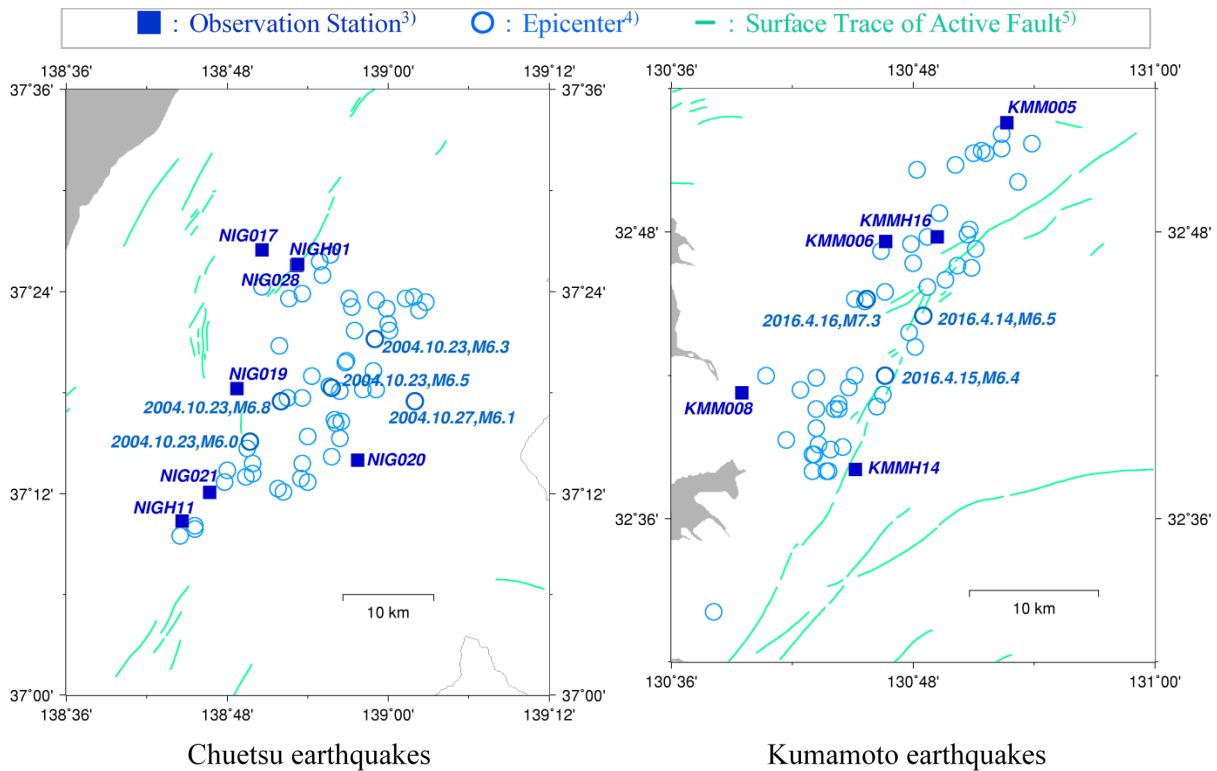


Fig. 2 Observation stations near the epicenters of the Chuetsu and Kumamoto Earthquakes and the epicenters of the earthquakes selected in this study

Thereafter, an analysis section spanning 60 s and common to the above mentioned three components was determined for the time history of every earthquake observation at each station to adequately shape the envelope. The analysis section was ascertained to exclude as many other smaller aftershocks as possible. Although the analysis section of 60 s may include other smaller aftershocks, with regard for the ultimate purpose of this study in reflecting the impact of the ground motion of the largest class in structural design, the omission of the aftershocks was considered unnecessary and thus maintained. Furthermore, cosine taper processing was applied to each of the first and last 2 s of the 60 s time history, and the obtained data were used for study.

Figure 3 illustrates three examples of the three-component acceleration time histories used in this study for the Chuetsu earthquake main shock ( $M$  6.8) and the Kumamoto earthquake main shock ( $M$  7.3). In each case, the large amplitudes were concentrated within a short period of around 10 s, and several waveforms with a maximum acceleration exceeding  $500 \text{ cm/s}^2$  were observed. At KMMH16 (Mashiki), the maximum acceleration of the EW component of the Kumamoto earthquake main shock exceeded  $1000 \text{ cm/s}^2$ .

First, the pseudo-velocity response spectra (hereinafter, referred to as “response spectra”) and the response duration time spectra<sup>6)</sup> of the ground motions of all the earthquakes were obtained for every component recorded at the observation stations to analyze the periodic characteristics of earthquake motions based on amplitude and duration. The response spectrum represents the maximum amplitude of the response time history for an input of the seismic motion in a single-degree-of-freedom system. Similarly, the response duration time spectrum corresponds to the duration in which the value of the normalized amplitude-squared accumulation curve of the same response time history is increased from  $p1$  to  $p2$ <sup>6)</sup>.

Table 1 List of observation stations and ground motion records in the near-fault regions of the Chuetsu and Kumamoto Earthquakes<sup>3), 4)</sup>

Chuetsu Earthquakes										Kumamoto Earthquakes							
Origin Time in 2004	<i>M</i>	Depth [km]	NIG 017	NIG 019	NIG 020	NIG 021	NIG 028	NIG H01	NIG H11	Origin Time in 2016	<i>M</i>	Depth [km]	KMM 005	KMM 006	KMM 008	KMM H14	KMM H16
10/23 17:56:00.3	6.8	13	○	○	○	○	○	○	○	04/14 21:26:34.4	6.5	11	○	○	○	○	○
10/23 18:03:12.6	6.3	9	○	○	○	○	○	○	○	04/14 21:41:03.4	4.0	12			○	○	○
10/23 18:07:30.9	5.7	15	○	○	○			○		04/14 22:07:35.2	5.8	8	○	○		○	○
10/23 18:11:56.7	6.0	12	○		○	○				04/14 22:16:08.7	4.1	6					○
10/23 18:19:24.0	4.2	2						○		04/14 22:38:43.5	5.0	11			○	○	
10/23 18:28:48.2	4.6	11		○			○			04/14 22:43:15.1	4.4	11				○	
10/23 18:34:05.6	6.5	14	○	○	○	○		○	○	04/14 23:28:13.6	4.4	13					○
10/23 18:36:50.9	5.1	7						○		04/14 23:29:58.1	4.6	13		○			○
10/23 18:44:34.2	4.2	14			○					04/14 23:43:41.1	5.1	14		○			○
10/23 18:54:35.4	4.7	8						○	○	04/15 00:03:46.4	6.4	7		○	○	○	○
10/23 18:57:26.2	5.3	8							○	04/15 00:34:17.1	4.5	13					○
10/23 19:01:05.6	3.8	14						○		04/15 00:53:01.5	3.9	12					○
10/23 19:07:32.6	4.3	10						○	○	04/15 01:53:01.4	4.8	12				○	○
10/23 19:36:45.9	5.3	11		○		○			○	04/15 05:10:36.8	4.6	10					○
10/23 19:45:57.1	5.7	12	○	○	○			○	○	04/15 07:29:55.9	4.2	12					○
10/23 19:55:18.6	3.9	11						○	○	04/15 07:46:52.0	4.4	11					○
10/23 20:02:40.0	4.3	9		○						04/15 23:17:31.6	3.6	7	○				
10/23 20:55:15.8	4.5	10							○	04/16 01:25:05.4	7.3	12	○	○	○	○	○
10/23 21:44:27.6	5.0	15			○			○	○	04/16 01:30:07.5	4.4	13			○	○	
10/23 22:28:18.2	4.2	15			○					04/16 01:44:07.4	5.4	15		○	○	○	
10/23 22:34:56.2	4.4	17			○					04/16 01:45:55.4	5.9	11	○	○	○	○	○
10/23 23:34:45.6	5.3	20	○		○			○		04/16 01:56:14.3	4.6	12					○
10/24 00:53:21.5	4.3	16	○					○		04/16 02:17:55.1	3.8	11	○				
10/24 09:28:04.0	4.8	12		○					○	04/16 04:05:49.2	4.0	12					○
10/24 10:06:00.3	4.5	10						○		04/16 04:34:23.7	3.4	6					○
10/24 10:29:18.3	4.1	15						○		04/16 04:51:24.5	4.3	14					○
10/24 14:21:34.9	5.0	11		○					○	04/16 07:23:54.3	4.8	12		○			○
10/24 16:06:31.8	4.6	12		○						04/16 08:02:48.3	3.8	10				○	
10/25 00:28:08.9	5.3	10		○						04/16 08:08:50.6	3.9	11	○				
10/25 01:27:52.4	4.7	6		○						04/16 08:20:41.5	4.6	12			○	○	
10/25 06:04:57.5	5.8	15	○	○	○			○		04/16 09:48:32.6	5.4	16	○	○	○		○
10/25 20:26:33.8	3.9	10		○						04/16 09:58:10.8	3.5	6				○	
10/27 04:15:23.5	3.6	6							○	04/16 10:26:10.4	3.8	11					○
10/27 10:40:50.2	6.1	12	○	○	○	○		○	○	04/16 10:38:53.1	4.5	10				○	
10/27 10:45:35.0	4.2	7						○		04/16 11:02:51.7	4.4	15		○			○
10/27 12:05:54.5	4.4	4	○					○		04/16 14:27:04.0	4.6	8			○	○	
10/27 15:23:21.7	4.0	2	○					○		04/16 16:02:01.0	5.4	12			○	○	
10/27 21:09:08.0	4.3	11			○					04/16 17:17:49.3	3.5	11	○				
10/29 10:27:32.0	3.6	9	○							04/16 18:25:10.7	4.0	10				○	
10/30 01:15:06.2	3.4	9							○	04/17 00:23:27.7	3.2	4				○	
11/01 04:35:49.1	5.0	8		○						04/17 04:46:49.0	4.5	10			○		
11/04 08:57:29.5	5.2	18	○	○				○	○	04/17 09:58:48.0	3.8	10				○	
11/06 02:53:21.3	5.1	0						○		04/17 11:51:35.1	3.4	5				○	
11/06 15:01:13.4	3.6	10							○	04/17 15:57:14.0	3.7	7				○	
11/08 11:15:58.5	5.9	0	○					○	○	04/17 19:23:41.2	4.4	11			○		
11/08 11:27:10.0	5.0	0						○		04/17 22:56:34.7	3.8	7				○	
11/08 11:32:17.2	5.1	6						○	○	04/18 08:35:43.0	4.2	10	○				
11/08 11:43:05.8	4.7	2						○		04/19 17:52:13.6	5.5	10				○	
11/10 03:43:08.3	5.3	5	○					○	○	04/28 12:56:32.5	3.7	9				○	
11/12 02:24:00.1	4.3	10			○					05/04 19:20:04.3	4.0	8					○
11/15 09:39:33.4	4.7	0						○		06/18 20:46:55.2	4.6	10			○	○	
12/23 21:03:43.3	4.5	11	○					○	○	Data used in this study							
12/28 18:30:36.8	5.0	8						○	○	10	11	13	26	24			

Major events ( Magnitude  $M \geq 6.0$  )  
 Proximal two stations ( in the vicinity of active faults )

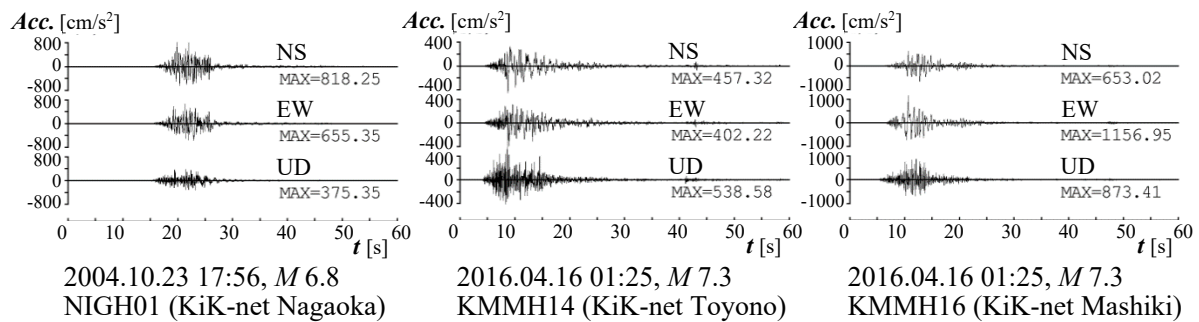


Fig. 3 Examples of acceleration time histories of ground motions in near-fault regions

Second, the response spectrum of ground motion was used as an index for estimating the response amplitude, and it was comparatively analyzed based on an engineering perspective with the maximum motion of the same component at the same site in the near-fault region of a series of earthquakes. Moreover, the largest response amplitude of a typical earthquake motion was analyzed for determining its predominance, in addition to the motions causing frequent occurrence of the largest response amplitudes. Moreover, the relative amplitudes of the ground motion responses resulting from other earthquakes were also examined. Among the earthquake motions selected for every component at each site, the values of the response spectra and their relative magnitudes varied depending on the period. Therefore, the response spectra of the selected earthquake motions were further analyzed by ranking the values obtained for each period.

Specifically, the values of the ground motion response spectra for all the target earthquakes were sorted in descending order for each site, component, and period. Thereafter, only the value with the highest rank in the order in each period, i.e., the largest response spectral value in each period, was selected for each site and component. It was then plotted on the vertical axis of the spectral diagram; the period was plotted on the horizontal axis. Similarly, the second and third ranks in the order were selected and displayed as spectral diagrams. The spectrum thus obtained is defined herein as the “sorted and ranked response spectrum.” Thus, the “first-ranked” sorted and ranked response spectrum displays the largest value among the ground motion response spectra for each site, component, and period, resulting from any of the serial seismic activities. Similarly, the “second-ranked” and “third-ranked” sorted and ranked response spectra are the second and third largest response spectra for each site, component, and period, resulting from any of the serial seismic activities.

Furthermore, the “ranked response spectral ratio” is defined as the sorted and ranked response spectrum of each rank divided by that of the first rank. Naturally, the first-ranked response spectral ratios are all valued at 1. The second-ranked response spectral ratio denotes the relative value of the second-largest ground motion response spectrum—for each site, component, and period, resulting from any of the serial seismic activities—to the value of the largest response spectrum. Thus, a second-ranked response spectral ratio of 1 would indicate that the largest response spectral value occurred at least twice during that period of serial seismic activity. Similarly, a second-ranked response spectral ratio of 0.5 would indicate that the response spectral values of subsequent ground motions were half or less than half of the largest response spectral value in that period of serial seismic activity.

The abovementioned examination results were analyzed to determine the applicability of the ranked response spectral ratio for building design and assessment in the future, and a modeling measure was proposed regarding the design and assessment of buildings against repeated strong motions.

### 3. RESULTS OF RESPONSE SPECTRA AND RESPONSE DURATION TIME SPECTRA

First, the pseudo-velocity response spectra  $pS_V$  [cm/s] and the response duration time spectra  $TS_V$  [s] were obtained with a 5 % damping factor for ground motions of all the target earthquakes at each site and component.

Figure 4 illustrates the pseudo-velocity response spectra  $pS_V$  (top) and velocity response duration time spectra  $TS_V$  (bottom) of the strong motions for the NS component of NIGH01 (Nagaoka) in the near-fault region of Chuetsu Earthquakes, the NS component of KMMH14 (Toyono), and the EW component of KMMH16 (Mashiki) in the near-fault region of Kumamoto Earthquakes, where the periods  $T$  [s] are plotted on the horizontal axes. The values evaluated in the previous study were adopted for the above-mentioned parameters  $p1$  and  $p2$ , which specify the beginning and end of the response duration:  $p1 = 0.03$  and  $p2 = 0.95$ , respectively<sup>6)</sup>. In addition, the spectra of all the targeted ground motions were overlaid, and the above-mentioned earthquakes with a magnitude  $M \geq 6.0$  are depicted with various colored lines.

In the  $pS_V$  of the NS component of NIGH01, the response amplitude of the  $M$  6.8 earthquake was the highest, whereas that of the  $M$  6.3 earthquake was slightly less, and that of earthquakes graded lower than five  $M6$ -class earthquakes were much less. The  $pS_V$  of the five large-scale earthquakes exhibited predominant periods of 0.3–2 s, and the response amplitudes in these periods attained maximum values

of approximately 100–200 cm/s. On the contrary, the  $pS_V$  for other earthquakes primarily displayed predominant periods of  $<1$  s, and the response amplitudes in these periods remained at 10–30 cm/s. Although certain  $TS_V$ s did not adequately eliminate other low-impact aftershocks, the response durations of the five large-scale earthquakes reached 20–40 s and were longer in the long-period range, which is evidently longer than the envelope of the acceleration time histories of the earthquake motions depicted in Fig. 3.

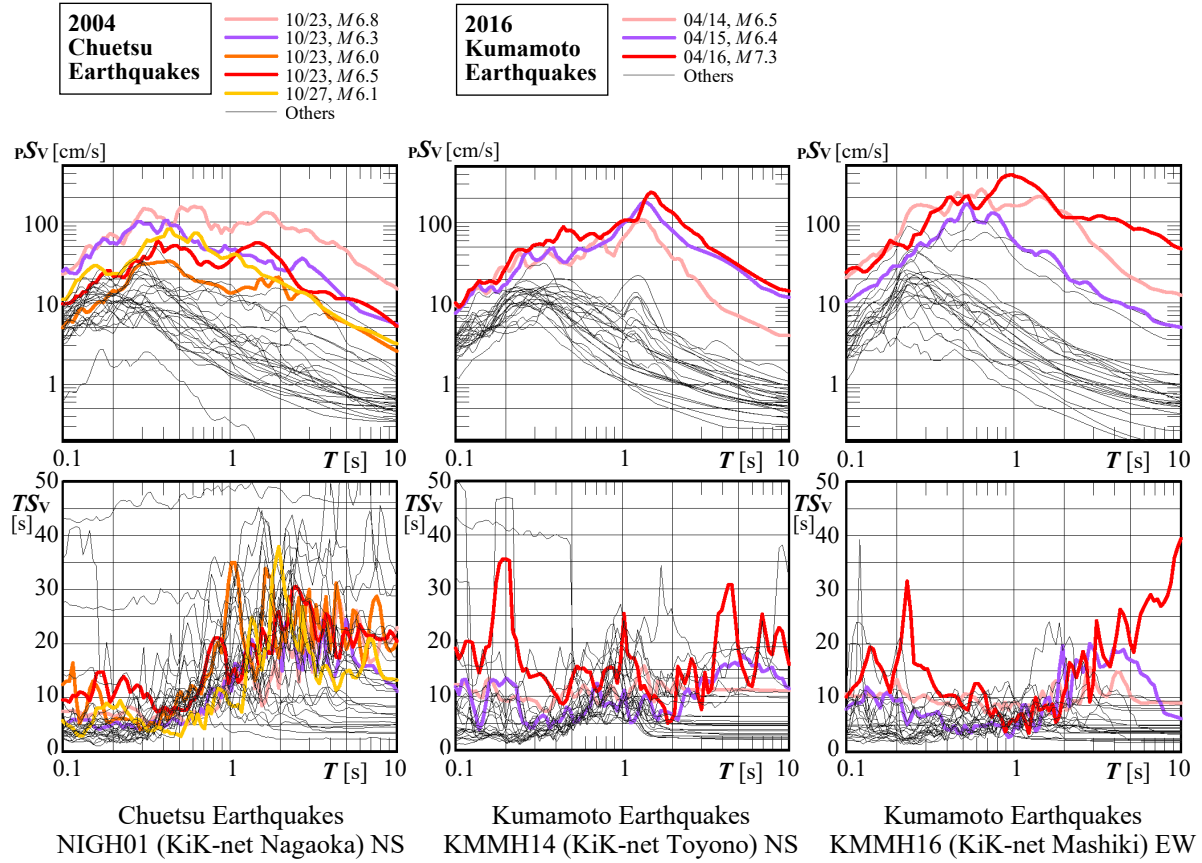


Fig. 4 Examples of pseudo-velocity response spectra  $pS_V$  [cm/s] and velocity response duration time spectra  $TS_V$  [s] of strong motions in near-fault regions of study sites (period  $T$  [s], damping factor  $h = 0.05$ , parameters  $p1 = 0.03$ ,  $p2 = 0.95$ )

In the  $pS_V$  of the NS component of KMMH14, the response amplitudes of the  $M 7.3$  earthquake and the  $M 6.4$  earthquake were the highest, whereas that of the  $M 6.5$  earthquake was almost equal in the short-period range but slightly low in the long-period range and that of the other earthquakes were much less. Moreover, the predominant periods of  $pS_V$  for the 3 large-scale earthquakes were 1–2 s with the response amplitudes in these periods escalating to 100–200 cm/s, whereas that for several other earthquakes were  $<1$  s with response amplitudes maintained at approximately 10–30 cm/s. Although certain  $TS_V$ s did not adequately eliminate the low-impact aftershocks, the response durations of the three large-scale earthquakes were relatively long compared to that of the others. In particular, this tendency was observed in the long-period range of the  $M 7.3$  earthquake.

In the  $pS_V$  of the EW component of KMMH16, the response amplitude of the  $M 7.3$  earthquake was the highest. The response amplitude of the  $M 6.5$  earthquake was equal to or larger than that with a period  $\leq 2$  s, but it was smaller than that with a period  $>2$  s. In addition, the response amplitude of the  $M 6.4$  earthquake was slightly low, and those of the other earthquakes were much lower. The predominant periods of  $pS_V$  for the three large-scale earthquakes were approximately 0.5–2 s with the response amplitudes in these periods ascending up to 100–400 cm/s. A major portion of the response spectra of

other earthquakes exhibited predominant periods of 0.2–0.5 s with the response amplitudes maintained at around several tens of centimeters per second. In  $TS_V$ , the response durations of the three large-scale earthquakes were relatively long, and this tendency was specific to the long-period range of the  $M$  7.3 earthquake.

Thus, the aforementioned recordings indicated that the largest response amplitude was generated in the near-fault region at least two or three times during the serial seismic activities; however, the intensity varied with the recording site, component, and period.

#### 4. RESULTS OF SORTED AND RANKED RESPONSE SPECTRA AND RANKED RESPONSE SPECTRAL RATIOS

The sorted and ranked response spectrum  ${}_pS_V^{#i}$  [cm/s] and the ranked response spectral ratio  $R^{#i}$  with a 5 % damping factor for all the target earthquakes were obtained for each station and component, where  $i$  indicates the rank (first to seventh), and  $R^{#i} = {}_pS_V^{#i}/{}_pS_V^{#1}$ .

Figure 5 presents the  ${}_pS_V^{#i}$  (top) and  $R^{#i}$  (bottom) for the NS component of NIGH01 in the near-fault region of Chuetsu Earthquakes, the NS component of KMMH14, and the EW component of KMMH16 in the near-fault region of Kumamoto Earthquakes, where each rank is depicted with various lines and the period  $T$  [s] is plotted on the horizontal axes. As mentioned above,  ${}_pS_V^{#i}$  is a descending sort index for the  ${}_pS_V$  values of all the target ground motions for each location, component, and period, which further displays the spectrum for each location and component. For instance, the top-left inset of Fig. 4 portrays the  ${}_pS_V$  of the NS component of NIGH01, where the value of the  $M$  6.8 earthquake (pink line) is almost the largest over the entire period, whereas the second-largest values are for the  $M$  6.5 earthquake (red line) near 1.5 s and the  $M$  6.3 earthquake (purple line) near 3 s, respectively. Focusing on the value of  ${}_pS_V^{#i}$  for each period in the top-left inset of Fig. 5, the first rank (green line) corresponds to the  $M$  6.8 earthquake (largest  ${}_pS_V$  component) depicted in Fig. 4, whereas the second rank (mint green line) corresponds to the second-largest value for each period in Fig. 4.

In  ${}_pS_V^{#i}$  of the NS component of NIGH01, the first rank spectrum was predominant in the period range of 0.3–2 s. On the contrary, the second-rank value maintained almost an equal value as compared to the first rank in a  $\leq 0.5$  s period but decreased slightly for long periods; the third and lower rank values gradually decreased as well. Naturally, the first-rank value of  $R^{#i}$  was 1. The second-rank value varied significantly depending on the period and was 0.9–1.0 at the maximum in the  $\leq 0.5$  s period, but the second-rank value dropped to  $\leq 0.6$  in the long-period range. Moreover, the values beyond that of the third rank were sequentially diminishing, and they were much lower in the  $< 0.4$  s period—most of them being  $< 0.6$ .

In  ${}_pS_V^{#i}$  of the NS component of KMMH14, the first rank spectrum was predominant in the period range of 1–2 s. The second-rank value was almost equal but decreased slightly. In addition, the third-rank value decreased slightly, primarily in the long-period range, and the values of the fourth and lower ranks gradually decreased thereafter. As for  $R^{#i}$ , the second-rank value varied significantly depending on the period, and the maximum was around 0.8–1.0. Although the third-rank value was large in the 1–2 s period or less, with the maximum at around 0.7–0.9, it was less than 0.4 in periods longer than 2 s. The values beyond the fourth rank decreased across the entire period and were  $< 0.2$  in periods  $\geq 1$  s.

In  ${}_pS_V^{#i}$  of the EW component of KMMH16, the first rank spectrum was predominant in the approximately 1 s period. The second-rank values decreased marginally in the short-period range but decreased significantly in the long-period range. Similarly, the third and lower rank values gradually decreased as well. Moreover, the second-rank values of  $R^{#i}$  varied significantly depending on the period; they were large at 0.8–1.0 in the  $\leq 2$  s periods and diminished to  $< 0.5$  in periods  $\geq 3$  s. In addition, the third-rank values were 0.5–0.8 in the  $\leq 1$  s periods, but it decreased to  $< 0.2$  in the  $\geq 2$  s periods. Furthermore, the values beyond that for the fourth rank were equal to or less than 0.5, even in the short period, and smaller in the long-period range.

Moreover, an abstraction and generalization is required to ensure the consideration of the above-mentioned characteristics for the utilizing the design at any site. Thus, it would be appropriate for the present author to use the acquired data for near-fault regions to compare with specific data analysis for

proximal stations, discuss, and organize the results of the study. In addition, the current author organized the results with attention to diversity, as the utilization policy for design varied with the target performance of the building.

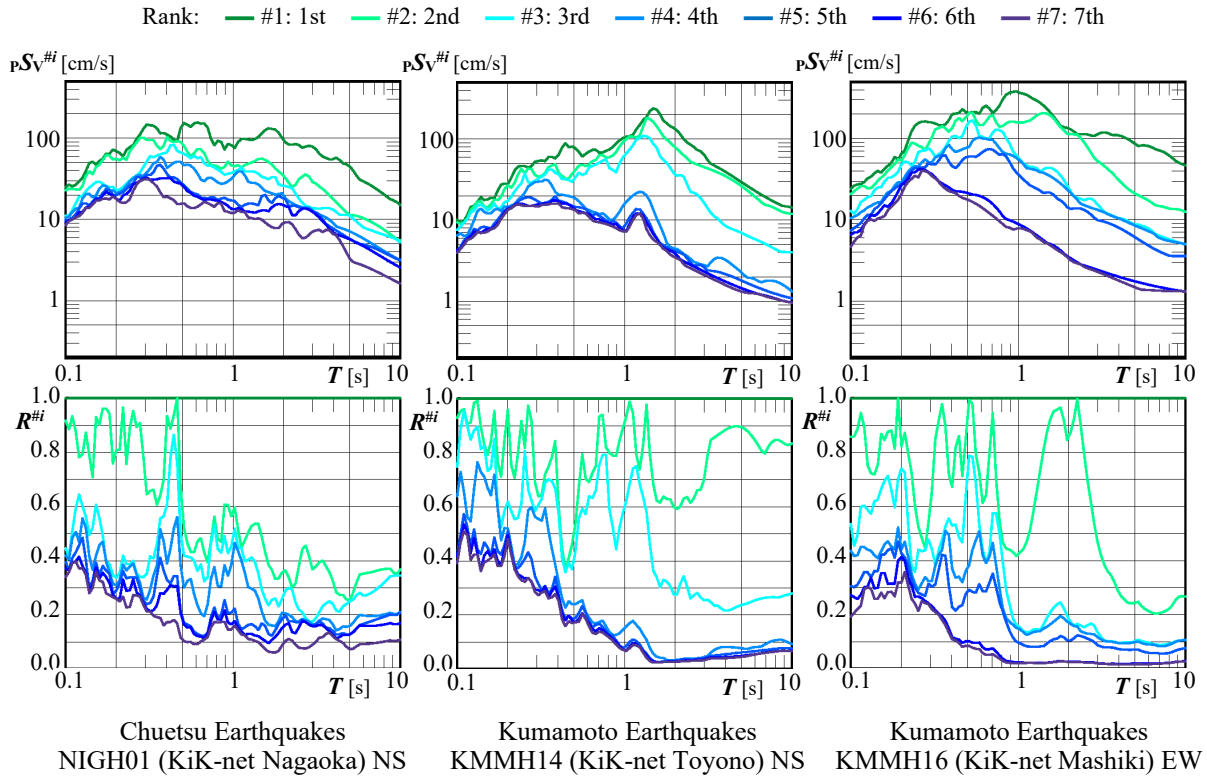


Fig. 5 Examples of sorted and ranked response spectra  $pSv^{#i}$  [cm/s] and ranked response spectral ratios  $R^{#i}$  of strong motions in near-fault regions ( $R^{#i} = pSv^{#i}/pSv^{#1}$ , rank  $i = 1$  to 7, period  $T$  [s], damping factor  $h = 0.05$ )

The ranked response spectral ratios  $R^{#i}$  of the second rank ( $R^{#2}$ ) and third rank ( $R^{#3}$ ) (because the first rank is self-evident) of strong motions detected for all the components of all the target stations in the near-fault regions: maximum value  $R_{MX}$ , average with standard deviation  $R_{AS}$ , average  $R_{AV}$ , standard deviation  $R_{SD}$ , and coefficient of variation (= standard deviation/average)  $R_{CV}$  are depicted in Fig. 6 with various lines. The left column of the figure portrays the combined results of all the 12 stations for both the seismic activities. The middle column presents the combined results of the five stations for the Kumamoto Earthquakes, during which fault displacement appeared on the ground surface. Lastly, the right column depicts the results for two stations (KMMH14 and KMMH16) located close to the fault of the Kumamoto Earthquakes. In addition, Fig. 7 illustrates the maximum value  $R_{MX}$ , average with standard deviation  $R_{AS}$ , average  $R_{AV}$ , standard deviation  $R_{SD}$ , and the coefficient of variation (= standard deviation/average)  $R_{CV}$  of the ranked response spectral ratios  $R^{#i}$  in each row, where the result of each rank is demarcated using various lines. The left column lists 12 stations for both the seismic activities, the middle column lists five stations for the Kumamoto Earthquakes, during which fault displacement appeared on the ground surface, and the right column lists two stations located close to the active faults of the Kumamoto Earthquakes.

The maximum values of  $R^{#i}$ ,  $R_{MX}$ , were around 1 in the second rank and within 0.9–1 in the third rank for the short period. However, it decreases for periods  $\geq 1.5$  s and becomes 0.4–0.5 in the long period of 10 s. Similarly, the  $R_{MX}$  for the fourth rank were within 0.7–0.9 in the short period but reduced to 0.1–0.4 in the long period of 10 s; thereafter, it gradually decreased for the lower ranks. The degree of reduction in the value owing to the descending rank was greater in the Kumamoto Earthquakes.

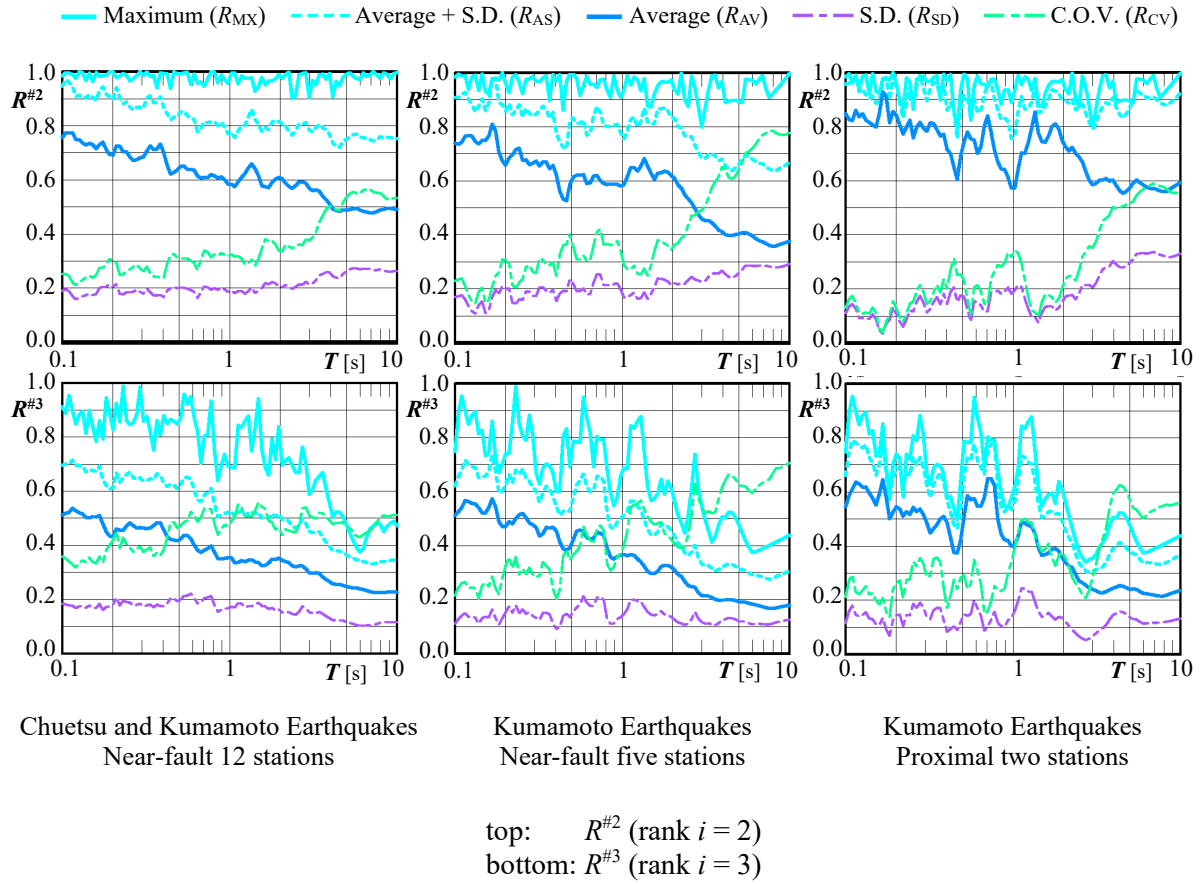


Fig. 6 Maximum value  $R_{MX}$ , average with standard deviation  $R_{AS}$ , average  $R_{AV}$ , standard deviation  $R_{SD}$ , and coefficient of variation  $R_{CV}$  of the ranked response spectral ratios  $R^{\#i}$  of strong motions for all the components at every target station in the near-fault region (period  $T$  [s], damping factor  $h = 0.05$ )

The average with standard deviation of  $R^{\#i}$ ,  $R_{AS}$ , of the second rank was around 1 at maximum but attained values  $\geq 0.9$  for periods  $\geq 2$  s. The maximum values for third rank were within 0.7–0.8 in the short periods but started to decrease from approximately 1.5 s and were reduced to 0.3–0.4 in the long period of 10 s, thereafter gradually decreasing for the lower ranks. Overall, the largest values were observed for the two stations located in the vicinity of the active faults of the Kumamoto Earthquakes.

The average of  $R^{\#i}$ ,  $R_{AV}$ , of the second rank was 0.8–0.9 at maximum for  $\leq 2$  s periods but decreased at  $\geq 2$  s periods and was reduced to 0.4–0.6 in longer periods of 10 s. For the third rank, the  $R_{AV}$  was 0.6–0.7 at maximum in the short periods, which decreased for periods  $\geq 1$  s and diminished to 0.2 for long periods of 10 s. Similarly, the maximum  $R_{AV}$  of the fourth rank was within 0.4–0.5 for short periods, which decreased for periods of 0.2 s and consequently deteriorated to approximately 0.1–0.2 for long periods of 10 s. Thereafter, the  $R_{AV}$  gradually decreased for further lower ranks. The largest values were observed for the two stations located in the vicinity of the active faults of the Kumamoto Earthquakes.

The standard deviation of  $R^{\#i}$ ,  $R_{SD}$ , of the second rank was 0.1–0.2 for short periods, which gradually increased to around 0.3 for long periods of 10 s. In addition, the  $R_{SD}$  for the third rank was around 0.1–0.2 and that for the fourth rank was 0.1–0.2 in the short period, which decreased from a period  $< 1$  s. Thereafter, the  $R_{SD}$  gradually decreased for further lower ranks. The largest values of  $R^{\#2}$  were observed in the long-period range for the two stations located in the vicinity of the active faults of the Kumamoto Earthquakes.

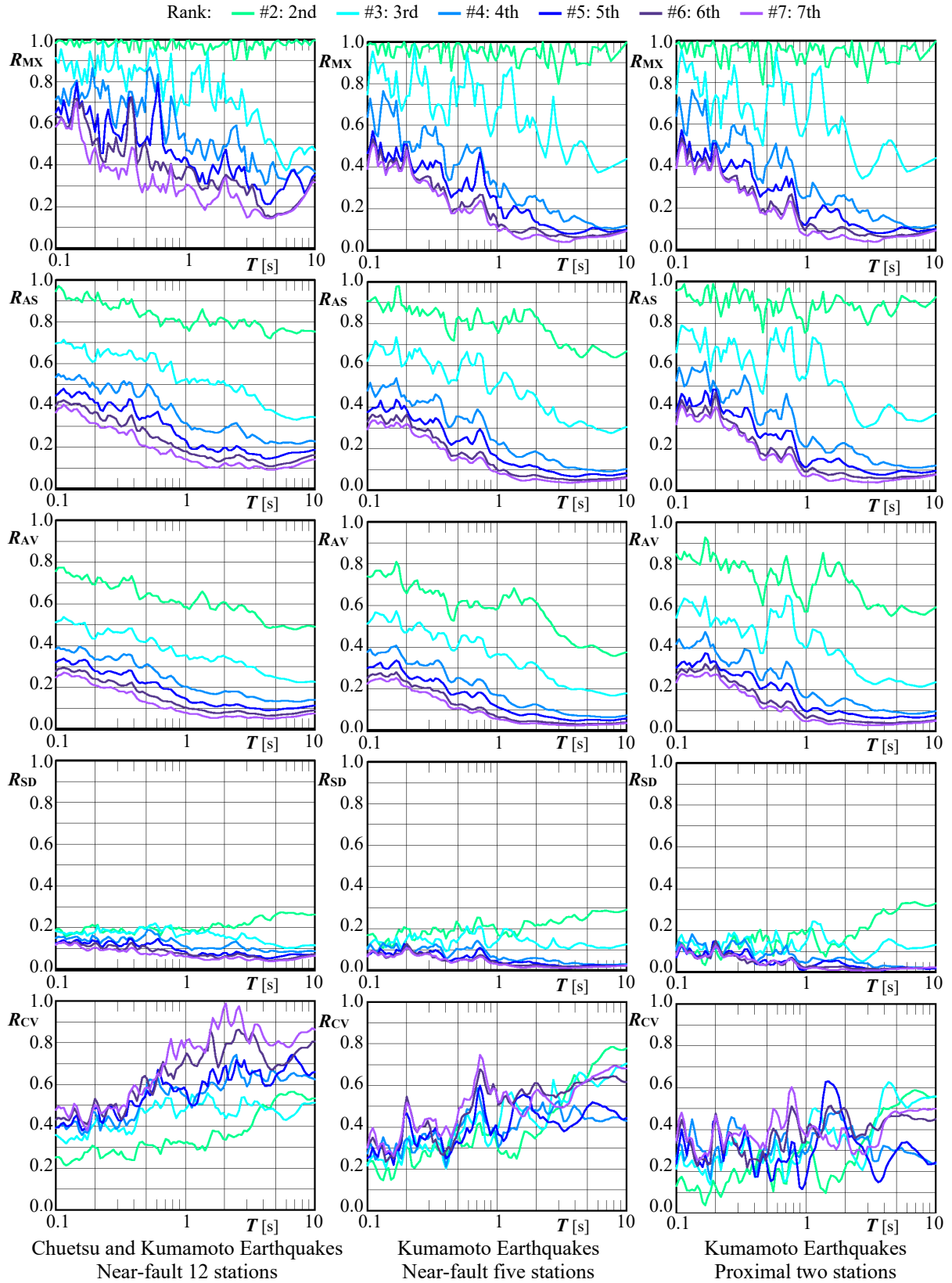


Fig. 7 Maximum value  $R_{MX}$ , average with standard deviation  $R_{AS}$ , average  $R_{AV}$ , standard deviation  $R_{SD}$ , and coefficient of variation  $R_{CV}$  of ranked response spectral ratios  $R^{#i}$  of all components at every target station in near-fault region (rank  $i = 2$  to  $7$ , period  $T$  [s], damping factor  $h = 0.05$ )

$R_{CV}$ , the coefficient of variation  $R^{#i}$ , is about 0.1–0.3 in the short periods in the second rank but gradually vary and increase with the periods and to be about 0.5–0.8 in the long period of 10 s, in the third rank are approximately 0.2–0.4 in the short periods but gradually vary and increase with the periods and to be 0.5–0.7 in the long period of 10 s, and in the fourth and lower ranks are almost same or a little more than these in the short period range but vary more depending on the period in the long period range.

## 5. DISCUSSION

Although the obtained ranked response spectral ratio  $R^{#i}$  exhibited peaks and valleys, fine peaks and valleys could vary depending upon marginal differences in the fault rupture properties, observation sites, and so on. Thus, the envelopes of spectra can be considered from an engineering perspective. In particular, the average with standard deviation of  $R^{#i}$ ,  $R_{AS}$ , was smaller than the maximum value,  $R_{MX}$ , but their overall tendencies correspond. In addition, the diversity and possibility of scenarios along with the selectively occurring phenomena in the near-fault regions suggest that the significance of the maximum value must be more important than that of the average value of  $R^{#i}$ . As  $R^{#2} \approx 1$  in this study, the earthquake motion causing the maximum class of response amplitude could be generated at least twice during a series of seismic activities. This study focuses on “the largest class series of strong motions in the near-fault region owing to a series of active crustal earthquakes that occur along the active faults.” Moreover, such phenomena selectively and inevitably occur under these limited conditions. Furthermore,  $R^{#3}$  displays a large value of approximately 1 in the short-period range, which decreases in the long-period range; this tendency can be observed for  $R^{#4}$  and lower ranks.

For sites close to an active fault system of a relatively simple shape, an exemplary scenario could be assumed for a pair of largest-class earthquakes occurring on the fault plane on both sides of the site, where each rupture directivity of an earthquake becomes the worst for the site. Therefore, even an extremely simple model can indicate that the worst-scenario earthquake will occur twice in a series of earthquakes, so  $R^{#2} \approx 1$  is normal.

In general, the standard deviation of  $R^{#i}$  decreased in the long-period range, but it increased in the long-period range for  $R^{#2}$ , and it fluctuated for  $R^{#3}$ . Notably, the coefficient of variation of  $R^{#i}$  tends to increase in the long-period range for  $R^{#2}$  and  $R^{#3}$ , regardless of the large periodic variation.

In general, the response spectrum of ground motion is larger for large-scale earthquakes, especially in the long-period range. Furthermore, there is a geometrical positional relationship in which the azimuth of the main rupture area on the fault plane is expected to alter significantly for even slight variations in the position of the observation station for near-fault regions. Therefore, the radiation pattern of the source and the rupture directivity of the asperity posed a significant influence, and the response amplitudes of the earthquake motions were considered to vary depending on the site and component, especially in the long-period range of 1–2 s or more. Accordingly, as discussed earlier, it is considered that the standard deviations of  $R^{#2}$  and  $R^{#3}$  did not decrease, and the coefficient of variation tended to increase in the long-period range. The current situation does not present sufficient information for specifying the asperity arrangement and rupture mode of future earthquakes in advance. Upon considering the strong motions occurring in the near-fault region, a scenario can be assumed, which poses an extremely significant influence of the radiation pattern and rupture directivity. As the maximum value of  $R^{#3}$  decreased in the long-period range, the contribution of rupture directivity was expected to decrease in the third rank than that for the first and second ranks.

On the contrary, the response amplitude of the ground motion in the short-period range would be large if an earthquake occurs within a short distance, regardless of the marginally smaller magnitude. Therefore, the degree of reduction in the value of  $R^{#i}$  based on the descending rank is smaller than that for the long-period range. During an aftershock activity, the frequency (number of times) of large response amplitudes caused by a series of earthquakes is higher in short-period structures than in long-period structures.

## 6. PROPOSED MODELING MEASURES OF STRONG GROUND MOTIONS FOR BUILDING DESIGN AND EXAMINATION

Based on the above-mentioned study results and their discussion, the ranked response spectral ratio was evaluated for application in structural design and assessments of buildings in future. Thus, a modeling measure is proposed herein for the design and assessment of buildings against repeated strong motions.

Currently, earthquake-resistant design and structural assessment, especially for extremely rare earthquake ground motions that occur in the near-fault region of crustal earthquakes, classify the largest class earthquake ground motion as a level 2 earthquake motion or an earthquake motion for examining structural margin which is sometimes referred to as a level 3 earthquake motion. In addition, dynamic earthquake response analysis of buildings is conducted. Therefore, the author utilized the ranked response spectral ratio  $R^{#i}$  in this framework and determined the extent and frequency of the repeating ground motions with respect to the set maximum earthquake ground motion.

As mentioned above, the envelope of the obtained  $R^{#i}$  poses engineering significance as its peaks and valleys vary based on conditions. In addition, the maximum value of  $R^{#i}$  is considered important because the variety and possibility of scenarios as well as the phenomena occurring selectively in the near-fault region are focused, and the findings at this instant were obtained from limited observations. Therefore, the maximum values of  $R^{#i}$  obtained from the 12 stations in the near-fault region with the highest amount of data were totally enveloped for analysis. However, different problems related to various performances excluding safety can be considered. Thus, the envelope value of the average with standard deviations of  $R^{#i}$  and the average of average values of  $R^{#i}$  were examined as well.

The ranked response spectral ratio  $R^{#i}$  that could be considered in the design and assessment of buildings are depicted in Fig. 8, where the maximum value  $R_{MX}$ , average with standard deviation  $R_{AS}$ , and the average  $R_{AV}$  of  $R^{#i}$  are presented. Six explanatory diagrams are presented in the top and middle rows, and the values obtained from analyzing the 12 stations in the near-fault regions are marked with dotted lines for each rank  $i$  (second to seventh). Furthermore, the proposals for envelope  $R_{MX}$  and  $R_{AS}$ , and the proposals for the average values of  $R_{AV}$  are depicted with alternating long and short dashed lines. The bottom row lists the proposals for  $R_{MX}$  on the left,  $R_{AS}$  in the center, and  $R_{AV}$  on the right.

Repeated earthquake ground motion can be determined by multiplying the response spectrum of the largest class ground motion as a level 2 earthquake motion or earthquake motion for margin examination or target response spectrum by the ranked response spectral ratio of the current proposal. Upon considering the response of the primary natural period of the building as excellent, the level 2 earthquake motion or the margin examination earthquake motion—set as the largest ground motion—can be substituted by multiplying the value of the ranked response spectral ratio of that natural period. Moreover, the order of the ranked response spectral ratio can be determined according to the problem under consideration. For instance, the same value can be realistically set below a certain rank to avoid unnecessary complexity. In general, the value of the ranked response spectral ratio converged at the seventh rank; thus, the value for the seventh rank can be set for the eighth and subsequent ranks. In addition, the duration varied with the ground motion, and the response duration time spectrum of the observation was longer for the largest class ground motion. Therefore, the proposed measure would induce a marginal duration time in the design and assessment of buildings during repeated occurrence of earthquake ground motions.

A specific example of creating an earthquake ground motion is presented for studying the impact of repeated strong motions with the application of this concept on the notification spectrum<sup>7)</sup> that is typically used for safety studies based on dynamic earthquake response analyses of buildings. First, the target response spectrum of the simulated ground motion of each rank was set by multiplying the notification spectrum<sup>7)</sup> of the extremely rare seismic motion (depicted in the top figure of Fig. 9) by each of the ranked response spectral ratio  $R^{#i}$  of the rank  $i$  (second to seventh), which is each  $R_{MX}$  depicted in the bottom left of Fig. 8 (the target response spectrum of the first rank is represented by the notification spectrum). For these target response spectra, the uniform random Fourier phase and Jennings' envelope function (where  $M$  adopts the largest scale in Table 1— $M$  7.3) were set, and the simulated earthquake ground motion was created with a data length of 60 s for each rank  $i$  (first to seventh). Moreover, the 7th rank ground motion was adopted for simulating ground motions in the eighth

to 10th ranks. A series of 10 rankwide connected ground motions in the near-fault region were obtained in order to examine the impact of serial active crustal earthquakes, as shown in the bottom figure of Fig. 9. In addition, the number of ranks of these earthquake ground motions can be set according to the structural characteristics and required performance of the target building or structure. Thus, this study proposed a validated approach that can positively reflect the impact of repeated strong ground motions in the performance-based design of structures. The current study presents an example of connecting the ground motions in descending order. However, the order of the ground motions can be altered (e.g., the maximum ground motion occurs at the end), depending on the purpose and content of the study.

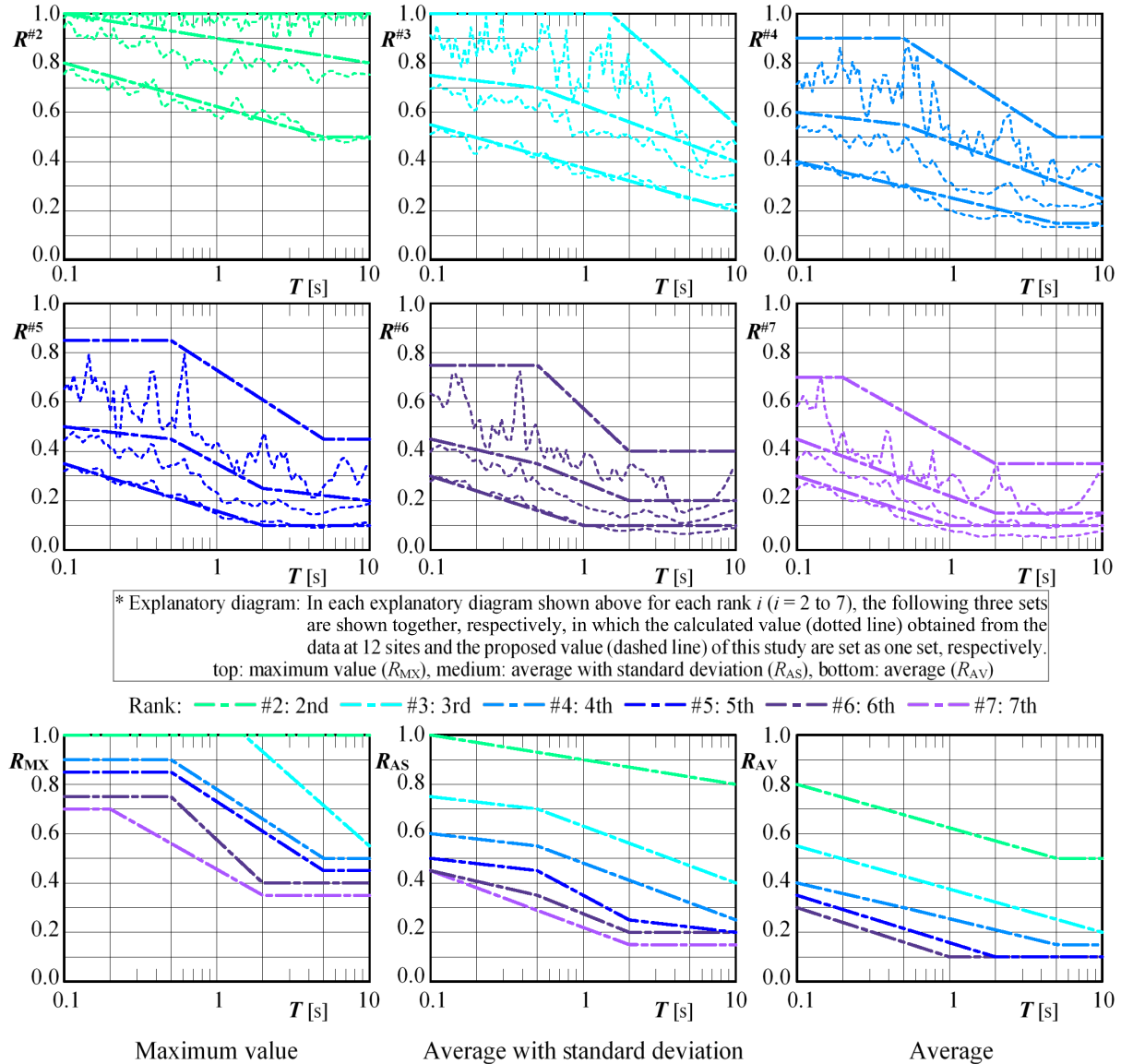
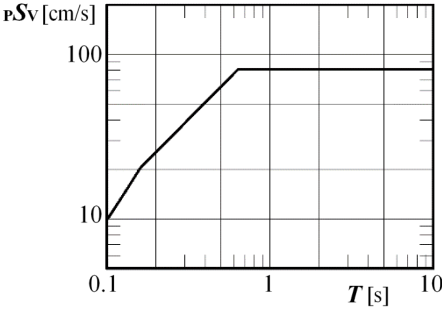


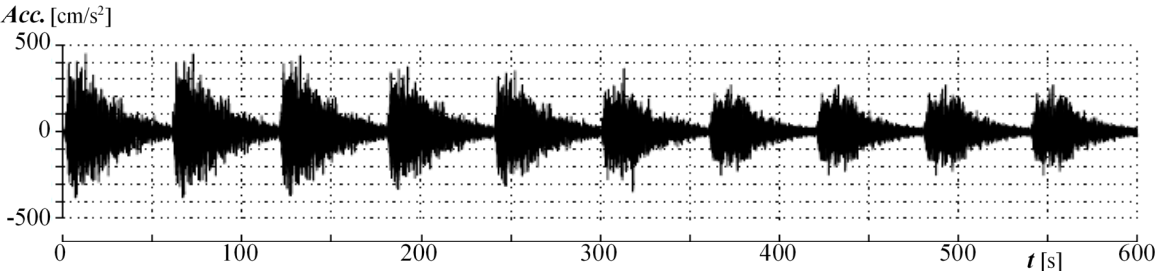
Fig. 8 Proposal of ranked response spectral ratios  $R^{\#i}$  considered in designing and examining buildings (rank  $i = 2$  to  $7$ , period  $T$  [s], damping factor  $h = 0.05$ )

As the response duration time spectrum of the observation was long in the largest earthquake motion, a margin will exist in the design and examination of the duration. This is a definite example for studying the impact of repeated strong motions with simulated ground motions created using a uniform random phase and Jennings' envelope function, which is often applied to actual design. In certain cases, the influence of surface waves cannot be ignored in a longer period range, and there may be various methods

for creating ground motions, including those providing phase characteristics of simulated ground motion and methods for expressing the duration.



Notification spectrum as the target response spectrum of simulated ground motion (earthquake motion that occurs extremely rarely)<sup>7)</sup>



Example of acceleration time history of simulated ground motion

Fig. 9 Example of creating ground motion for studying impacts of repeated strong motions in near-fault region of a series of active crustal earthquakes

As this study utilized rare observations in the near-fault regions of crustal earthquakes with extremely active aftershock activities, the presented proposal is theoretical, and the absolute values should be reviewed as necessary and verified with future earthquakes.

**7. CONCLUSIONS**

Among the surface ground motion records of the Chuetsu and Kumamoto Earthquakes observed in the recent years, the ground motion records at 12 stations in the near-fault region, including two stations located close to the active fault during a series of active crustal earthquakes were analyzed. The pseudo-velocity response spectra and response duration time spectra of the ground motions were examined. In addition, the sorted and ranked response spectra and ranked response spectral ratio were originally defined in this study to determine the actual state of strong motions in the near-fault regions for analysis. In particular, the strong motions that cause the highest response amplitude could be generated at least twice in the near-fault region, and the frequency (number of times) of large response amplitudes are relatively higher in short-period structures than in long-period structures owing to a series of aftershock activities. Furthermore, the ranked response spectral ratio was utilized to propose a modeling method for repeated strong ground motions and determine the intensity and frequency of ground motions that should be set for the largest ground motion in the design and assessment of buildings.

The results of this study are expected to support the ingenuity and ideas of careful but ambitious practitioners of performance-based design. In this study, the author proposed a strong motion measure for studying the impact of repeated strong motions via sorted and ranked response spectra from the perspective of earthquake ground motion for applicability in the performance-based design of buildings and structures. Moreover, the tolerable behavior, response, and damage are required for evaluation based on the specific structural characteristics and desired performance of the building or structure. Thus, an

applicable measure can be generalized for designing buildings and structures in the future, if an adequately advanced assessment is conducted from both the perspective of ground motion and building response and societal consensus is obtained.

As this study was first realized by utilizing rare observation records obtained at near-fault regions of only the two activities of crustal earthquakes with extremely active aftershock activities observed in the past years, the generality of the current conclusions should be verified for adequate. Currently, the content is summarized from the perspective of possible measures, considering at least the knowledge obtained from the Chuetsu and Kumamoto Earthquakes that actually occurred. In the future, more information will be necessary, in terms of observing the largest class ground motions multiple times in the near-fault region of a large earthquake with extremely active aftershock activity.

The Chuetsu earthquakes analyzed in this study exhibited unclear relationships with the nearby active faults<sup>1)</sup>, whereas the Kumamoto Earthquakes that occurred along the active fault zone mainly contained strike-slip components including normal fault components<sup>2)</sup>. Although sufficient data are unavailable presently, there are still challenges with examining the earthquakes occurring along the reverse fault-type active faults and highly complex active faults: for instance, the value of  $R^{#3}$  may be even larger and increase to almost 1. In addition, a subduction-zone huge earthquake is a large-scale earthquake that causes strong ground motions over a wide area. Generally, a majority of areas near a subduction-zone earthquake fault is an oceanic region. However there are also examples of large earthquakes occurring along the Sagami Trough or the Suruga Trough, in which the land areas are included just above the source faults. Thus, a similar analysis as that conducted in this study will be necessary for future earthquakes.

## ACKNOWLEDGMENT

The current study utilized earthquake information from the Japan Meteorological Agency and the public data from the strong motion observation network of the National Research Institute for Earth Science and Disaster Resilience. In addition, the generic mapping tools (GMT) were used to create the epicentral distribution map. The author would like to thank Dr. Sachie Kotsuki of Shimizu Corporation for her cooperation in creating the simulated ground motions, anonymous reviewers for their valuable opinions on the manuscript, and Editage ([www.editage.com](http://www.editage.com)) for English language editing. (Certain portions of this study were published in References 8 to 11.)

## REFERENCES

- 1) The Earthquake Research Committee of the Headquarters for Earthquake Research Promotion: Evaluation of Seismic Activities in Chuetsu Region, Niigata Prefecture, 2004 (in Japanese).
- 2) The Earthquake Research Committee of the Headquarters for Earthquake Research Promotion: Evaluation of the 2016 Kumamoto Earthquakes, 2016.
- 3) National Research Institute for Earth Science and Disaster Resilience: Strong-Motion Seismograph Networks (K-NET, KiK-net). <https://www.kyoshin.bosai.go.jp/> (last accessed on August 10, 2018)
- 4) Japan Meteorological Agency: Earthquake Information (Earthquake and Seismic Intensity Information). [http://www.jma.go.jp/en/quake/quake\\_singendo\\_index.html](http://www.jma.go.jp/en/quake/quake_singendo_index.html) (last accessed on August 10, 2018)
- 5) Nakata, T. and Imaizumi, T.: *Detailed Digital Map of Active Faults*, University of Tokyo Press, 2002 (in Japanese).
- 6) Ishii, T.: Response Duration Time Spectra of Earthquake Ground Motions, *Journal of Structural and Construction Engineering (Transactions of AIJ)*, Architectural Institute of Japan, Vol. 77, No. 676, pp. 843–850, 2012 (in Japanese with English Abstract).
- 7) Ministry of Construction: Establishing Structural Calculation Standards to Confirm the Safety of the Structural Strength of Skyscrapers, Ministry of Construction, Notification No. 1461, 2000 (in Japanese).

- 8) Ishii, T.: A Study on Near-Fault Strong Ground Motions During the 2016 Kumamoto Earthquakes, *Programme and Abstracts, 2017 Fall Meeting*, The Seismological Society of Japan, S15-04, 2017 (in Japanese).
- 9) Ishii, T.: A Study on the Effects of Near-Fault Strong Ground Motions During the 2016 Kumamoto Earthquakes, *Proceedings of the 13th Annual Meeting of Japan Association for Earthquake Engineering*, P1-8, 2017 (in Japanese).
- 10) Ishii, T.: A Study on Near-Fault Strong Ground Motions Which Occurred Frequently During the 2016 Kumamoto Earthquakes, *Proceedings of the Annual Meeting of Architectural Institute of Japan*, pp. 591–592, 2018 (in Japanese).
- 11) Ishii, T.: Investigation on Near-Field Strong Motions Occurring Frequently During Active Series of Crustal Earthquakes, *Proceedings of the 15th Japan Earthquake Engineering Symposium*, pp. 2478–2487, 2018 (in Japanese with English Abstract).

**(Original Japanese Paper Published: November, 2020)**

**(English Version Submitted: March 23, 2021)**

**(English Version Accepted: April 14, 2021)**